Chinese Journal of Chemical Engineering 26 (2018) 1803–1813

Contents lists available at ScienceDirect

Chinese Journal of Chemical Engineering

journal homepage: www.elsevier.com/locate/CJChE

Article

Hydrodynamics features of dispersed bubbles in the ventilated wake flow of a cylinder☆

Ning Mao [1], Can Kang [1,*], Wisdom Opare [1,2], Yang Zhu [1]

[1] School of Energy and Power Engineering, Jiangsu University, Zhenjiang 21213, China
[2] Faculty of Engineering, Takoradi Technical University, Takoradi, P.O. Box 256, Ghana

ARTICLE INFO

Article history:
Received 28 June 2017
Received in revised form 26 March 2018
Accepted 7 April 2018
Available online 18 April 2018

Keywords:
Bubble
Ventilation
Wake flow
PIV
Photography
Bubble size distribution

ABSTRACT

An experimental study was conducted to investigate the 2D bubbly flow downstream of a cylinder. Sparsely distributed bubbles were produced using the ventilation method. The carrier flow was measured using the particle image velocimetry (PIV) technique. The shadow imaging technique was used to capture instantaneous bubbly flow images. An image-processing code was compiled to identify bubbles in acquired image, calculate the bubble equivalent diameter and the bubble velocity. The effects of Reynolds number and the flow rate of the injected air were considered. The result indicates that the carrier flow is featured by distinct flow structures and the wake region is suppressed as the upstream velocity increases. Regarding the bubbles trapped in the wake flow, the number of small bubbles increases with the upstream velocity. On the whole, the bubble velocity is slightly lower than that of the carrier flow. The consistency between small bubbles and the carrier flow is high in terms of velocity magnitude, which is justified near the wake edge. The difference between the bubble velocity and the carrier flow velocity is remarkable near the wake centerline. For certain Reynolds number, with the increase in the air flow rate, the bubble equivalent diameter increases and the bubble void fraction is elevated.

1. Introduction

Bubbly flows facilitate the heat and mass transfer between different phases and therefore assume an important function in chemical and environmental engineering [1–3]. Fundamentally, the inter-phase interaction involved in the bubbly flow depends significantly on both bubble parameters and the traits of the carrier flow. Some bubbly flows are characterized by scattered bubbles. In this context, the deviation of bubble behavior from general pseudo-single phase model is appreciable. At present, regarding the available knowledge of the bubbly flow, empirical relationship instead of quantitative conclusions is prevalent. Bubbles trapped in liquid flow are subjected to the influence of multiple factors such as gas volume fraction, liquid density and flow parameter distribution. An accurate acquisition of bubble size and its spatial distribution enables the understanding of bubble dynamics under specific flow conditions. Meanwhile, the identification of bubbles is a prerequisite for tracing the essence of the carrier flows, particularly the flows featured by high velocity gradients and strong turbulence.

Non-intrusive flow measurement and visualization techniques, such as X-ray technique and high speed photography (HSP) [4–8], lend sound support in bubbly flow research. Kong *et al.* [9] used the γ-CT measurement technique to investigate the gas content in the gas–liquid two-phase flow stirred by a Rushton rotor, and the influence of ventilation position and air flow rate on the gas content was explained. Shollenberger *et al.* [10] used γ-ray to measure bubble rising behavior at different air flow rates. X-ray tracking particle velocimetry (XPTV) was employed by Seeger *et al.* [11] to measure the flow field in the bubble column at high air void fraction and both flow field characteristics and cross-sectional air content were presented. Xu *et al.* [12] used ultrasonic tomography to detect instantaneous phenomena in the gas–liquid two-phase flow and developed a real-time monitoring system. High speed photography (HSP) serves as another useful tool in the study of the gas–liquid two-phase flow. Triplett *et al.* [13] depicted the gas–liquid two-phase flow pattern based on image processing technology. With particle image velocimetry (PIV), Hernandez-Alvarado *et al.* [14] measured bubble void fraction, bubble size and interfacial area in co-current downflow bubble column reactor using HSP. Image processing techniques are critical for extracting information from captured images. Lau *et al.* [15] attempted to separate overlapping bubbles in bubbly flows with large void fraction by means of a watershed algorithm. These studies take the understanding of bubbly flow to a new height. With the development of bubbly flow measurement and visualization techniques, the amount of data has been enhanced considerably. In this context, measurements of high quality deserve more attention. Nevertheless, studies in this aspect are rather limited hitherto.

☆ Supported by the National Natural Science Foundation of China (51676087).
* Corresponding author.
E-mail address: kangcan@mail.ujs.edu.cn. (C. Kang).

https://doi.org/10.1016/j.cjche.2018.04.002
1004-9541/

The purpose of the present study is to seek bubbly flow characteristics in the wake flow downstream of a cylinder. An experimental work is conducted with the cylinder deployed in the 2D test segment of a water tunnel. Bubbles are produced with a ventilation device installed upstream of the cylinder. The emphasis is placed on the bubbles entrapped in the wake flow downstream of the cylinder. Under the condition of no ventilation, the pure water flow downstream is measured using PIV. With ventilation, the bubbly flow in the wake of the cylinder is visualized with the shadow imaging technique, and then the bubble images acquired are processed with an in-house code. Statistics on the bubbles are extracted from consecutive images. The influence of the upstream velocity and the air flow rate on bubble size and bubble kinematic characteristics is investigated.

2. Experimental

2.1. PIV measurement set-up

A particle image velocimetry system manufactured by LaVision Company of Germany was used in the experiment. The PIV system is composed of a low-frequency double-pulse laser, a CCD camera with the double-frame and double-exposure modes, a time synchronization controller, a set of laser beam guiding arms and lenses, and Davis software for data acquisition and process. The configuration of primary components of the PIV experiment is displayed in Fig. 1. Hollow glass particles, with diameters ranging from 20 to 50 μm, served as tracing particles in the experiment. The depth of view (DOV) plane for the measurement was set to overlap with the mid-span plane of the cylinder. According to the operation parameters of the camera, the depth of view was 8.1 mm. In this context, the monitored zone is sufficiently thick to accommodate the moving bubbles.

2.2. Water tunnel test segment and cylinder

The experiment was carried out based on the platform of a water tunnel, and the attainable water flow velocity with this water tunnel is 13 $m \cdot s^{-1}$. In the present study, upstream velocities of 1.25 $m \cdot s^{-1}$, 1.61 $m \cdot s^{-1}$, 1.98 $m \cdot s^{-1}$, 2.35 $m \cdot s^{-1}$ were selected. The characteristic length was defined as the width of the test segment, so the corresponding Reynolds number, *Re*, are 37425, 48203, 59281, and 70060, respectively. The test segment illustrated in Fig. 2, with dimensions of 700 mm (length) × 50 mm (width) × 350 mm (height), is made from plexiglass and used to accommodate the cylinder. The height *H* and diameter *D* of the cylinder are 50 mm and 30 mm, respectively. Therefore, the block ratio of the test segment is 0.086. The flow region monitored with PIV is shown in Fig. 2 as well.

A convergent segment is mounted upstream of the test section and the profile of this segment conforms to the Witozinsky curve, and connects the stabilization segment with identical cross sections of 390 mm × 390 mm and the inlet of the test section (315 mm × 50 mm). To examine the influence of the test section geometry on velocity distributions, PIV measurement was conducted with the cylinder removed. Velocity profiles at various Reynolds numbers are plotted in Fig. 3. Through changing the optical configuration, the velocity distributions in both *xoy* and *xoz* planes were obtained. Along *y* direction, namely the height of the test section, obvious velocity gradients occur near the upper and lower walls of the test section. In the middle part, the velocity distributions are rather uniform, as shown in Fig. 3(a). Along *z* direction, similar velocity distribution tendencies are demonstrated. The shape of the velocity profile is insensitive to the variation in Reynolds number; therefore, high quality of the carrier flow eliminates the disturbance of unexpected factors on the bubbles that would be involved.

2.3. Shadow imaging system

In view of the deficiency of PIV in studying scattered bubbles, shadow imaging technique was used here to acquire bubble information. This technique is based on backlight illumination and the high-magnification imaging. The shadow of bubbles in the focal plane of the optical lenses is recorded. Relative to PIV, the sheet light source of PIV is replaced with the volumetric light source; moreover, the rigid laser arm is replaced with the flexible optical fiber. The schematic view of the shadow imaging system and the major facilities are shown in Fig. 4. A CCD camera with the double frame and double exposure shooting mode was used to capture consecutively bubble images. The depth of view plane was geared to the midspan plane of the test section. The dimensions of the monitored area are $3D \times 2D$. The window size depends on the image resolutions and the accuracy of bubble edge detection. Considering the bubbly flow downstream of the cylinder, as shown in Fig. 2, such a window is advantageous for observing the influence of the wake on bubbles. The acquisition frequency is 6.9 Hz, and each data group was composed of 200 instantaneous images. For each Reynolds number, the final results were averaged based on three data groups.

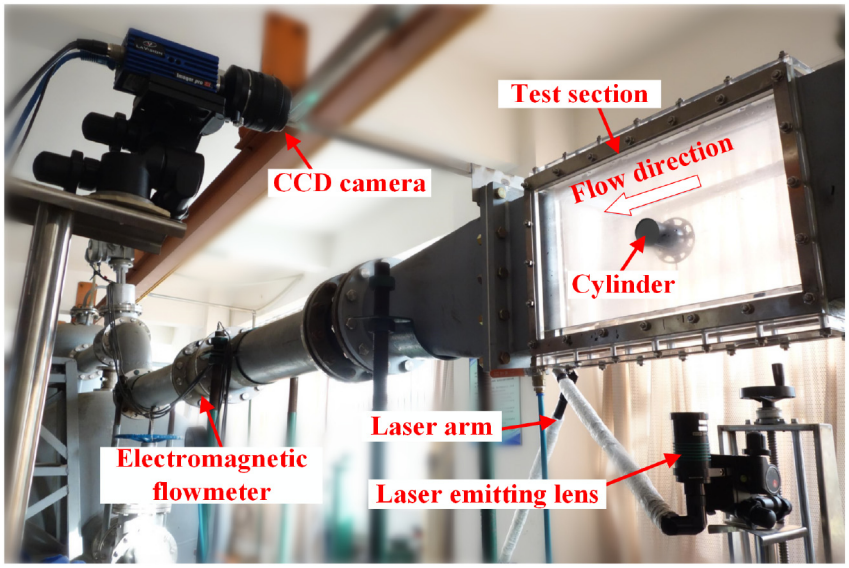

Fig. 1. Primary components of the PIV experiment rig.